Probing the Kinetics of a Nonadiabatic Transition Initiating Out of Vibrationally Excited as Well as Ground State Modes with Femtosecond Time-Resolved Transient Gratings†

ARTICLE *in* THE JOURNAL OF PHYSICAL CHEMISTRY A · SEPTEMBER 2003

Impact Factor: 2.69 · DOI: 10.1021/jp022650q

5 AUTHORS, INCLUDING:

Arnulf Materny
Jacobs University
198 PUBLICATIONS **2,328** CITATIONS
SEE PROFILE

Wolfgang Kiefer
University of Wuerzburg
878 PUBLICATIONS **9,837** CITATIONS
SEE PROFILE

Probing the Kinetics of a Nonadiabatic Transition Initiating Out of Vibrationally Excited as Well as Ground State Modes with Femtosecond Time-Resolved Transient Gratings†

T. Siebert, V. Engel, A. Materny,‡ W. Kiefer, and M. Schmitt*

Institut für Physikalische Chemie der Universität Würzburg, Am Hubland, D-97074 Würzburg, Federal Republic of Germany

Received: December 31, 2002; In Final Form: May 16, 2003

Femtosecond time-resolved population gratings are employed for observing the kinetics of vibrational cooling and internal conversion in the S_1 state of β-carotene. Two independent laser pulses, which are tuned resonant to the $S_2 \leftarrow S_0$ optical transition induce transient population gratings into solutions of β-carotene. Because the S_2 state lies approximately 6000 cm^{-1} above the S_1 potential, the subsequent internal conversion to the S_1 state generates a population grating of hot vibrational modes on the S_1 potential. This is followed by vibrational cooling and an internal conversion to the electronic ground state. The kinetics associated with these processes are interrogated by scattering a third, time-variable probe pulse off the S_1 state population gratings under Bragg conditions. When the probe laser pulse is tuned to different wavelengths within the red flank of the $S_n \leftarrow S_1$ absorption profile, excited vibrational states as well as the vibrational ground state modes in the S_1 potential can selectively be monitored. This is verified by characterizing the contribution of vibrational cooling to the acquired kinetics. With a comparison between the kinetics observed for excited and ground state vibrational modes, it can be shown that the rate of the S_1/S_0 internal conversion increases for hot vibrational modes.

1. Introduction

Since the beginnings of quantum theory, a better understanding of the vast complexity innate to polyatomic molecules has been the aim of numerous works.[1−3] Particularly interesting is the coupling between nuclear and electronic motion, which governs elementary aspects of photochemistry and photobiology.[4−11] Here, nonadiabatic coupling determines the pathway of photochemical reactions such as electron transfer, photodissociation, and photoisomerization, thereby taking a central role in the mechanism of highly efficient photobiological processes such as vision and photosynthesis.[12−15] The electronic transitions and nuclear dynamics involved in these processes take place on an ultrafast time scale, and it is the progress in laser technology, opening the possibility of laser spectroscopy with femtosecond (fs) time resolution, that allows for the direct observation of coupled electronic and atomic motion in real time. The new insight into the dynamic aspects of molecules observed on the relevant time scale has brought great advances to the field of molecular physics.[16−18]

On the ultrafast time scale, third-order, optical spectroscopy has shown the capability to address many facets of molecular dynamics due to the numerous degrees of freedom innate to this type of spectroscopic method.[9,19−21] Fundamental contributions in the area of coherent four-wave mixing (FWM) spectroscopy were made by Albrecht and co-workers. They used both theory and experiment to examine problems of photophysical and photochemical interest in nonlinear light-matter interactions (see, e.g., refs 22−24).

The experiments presented in this work explore the S_1/S_0 internal conversion (IC) in β-carotene with special emphasis on the influence of the vibrational energy of modes engaging in this radiationless electronic transition. It is the electronic structure of β-carotene and other carotenoids that allows this molecule to fulfill a variety of essential functions in the process of photosynthesis.[14,25,26] The close proximity in energy of the two lowest excited singlet states, denoted S_1 and S_2 in β-carotene to the Q_x and Q_y bands of chlorophyll A and B, allow for energy transfer between these two types of molecules via dipole/dipole coupling an electron exchange mechanisms. In photosystem II, one of the light harvesting units in photosynthesis, β-carotene and chlorophyll systems act as the active chromophors. Here, the spatial proximity of these two types of molecules, together with the possibility of an energy exchange, allows β-carotene and related carotenoids to act as (i) auxiliary light-harvesting pigments, with energy transfer to chlorophyll molecules, (ii) dissipators of excess photoenergy collected by chlorophyll units, (iii) photoprotectors via the quenching of chlorophyll triplet states, and (iv) scavengers of singlet oxygen.[26] The S_1/S_0 internal conversion in β-carotene plays an important role in regulating all these elementary reactions. This process, which is initiated by the S_2/S_1 internal conversion, has been studied by Albrecht et al. and other groups by means of transient absorption spectroscopy.[27−31]

In the present work, the method of femtosecond time-resolved transient grating spectroscopy is applied to the study of the S_1/S_0 internal conversion. By employing this method, we seek to utilize the innate sensitivity of FWM technique to the population dynamics in the system of interest. The sensitivity is given by the nature of the FWM signal which, under the proper phase matching conditions, allows for a background free detection of a directed coherent signal. This is in contrast with the commonly applied technique of transient absorption, which inherently

† Part of the special issue "A. C. Albrecht Memorial Issue".

* Author for correspondence. Email: mschmitt@phys-chemie.uni-wuerzburg.de. Fax: +49-931-888-6332. Phone: +49-931-888-6338.

‡ Present address: School of Engineering and Science, International University Bremen, P.O.Box 750 561, D-28725 Bremen, Germany.

10.1021/jp022650q CCC: $25.00
Published on Web 09/06/2003

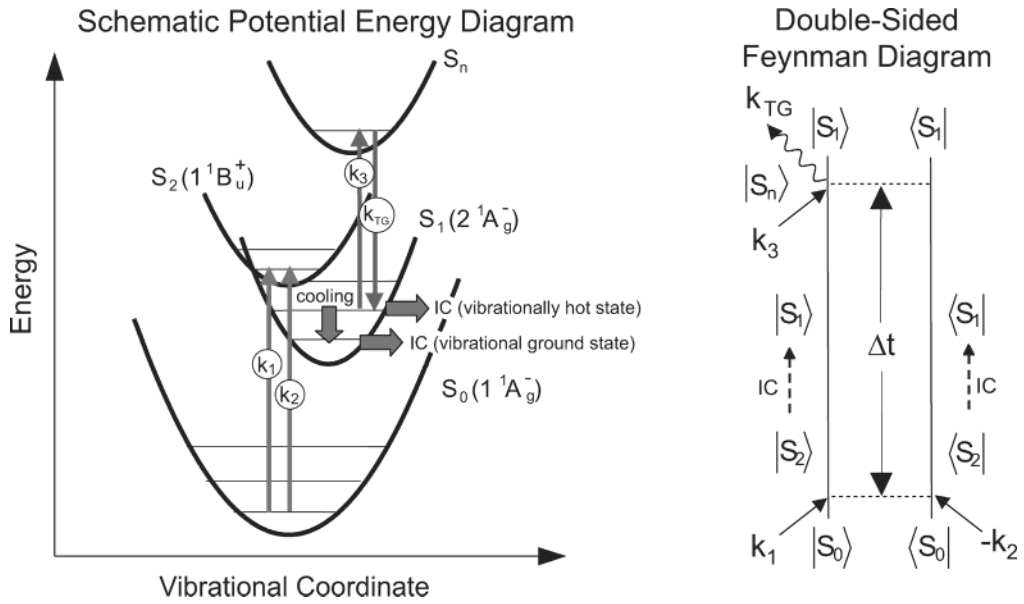

Figure 1. Schematic Potential energy diagram of β-carotene (left) and the double-sided Feynman diagram (right) illustrating the transient grating technique used to determine the kinetics of the S_1/S_0 internal conversion initiating out of vibrationally excited as well as ground state modes. Two pump lasers (**1** and **2**, $\lambda_{pu} = 510$ nm, fwhm = 70 fs, 60 nJ), induce a population grating of electronically excited molecules in the S_2 state of β-carotene. The subsequent S_2/S_1 internal conversion populates the S_1 state that is probed by elastically scattering a third probe pulse (**3**, $\lambda_{pu} = 570-660$ nm, fwhm = 70 fs, 60 nJ) off the population grating, generating the coherent signal **4** (k_{TG}) in the phase-matched direction. The probe pulse is delayed variably in time (Δt) relative to the two laser pump pulses that interact simultaneously with the sample to induce the population grating. The probe pulse is tuned variably to be in resonance to the $S_n \leftarrow S_1$ optical transition and furthermore spectrally red-shifted out of this optical transition to enhance the interrogation of vibrationally excited states in the S_1 potential.

requires the detection of a small absorption difference carried on a large stationary background. Furthermore, the transient grating technique does not require the use of a reference that is subtracted from the transient signal. This increased sensitivity allows for the kinetics of different vibrational quantum states to be differentiated, opening the possibility to characterize the contribution of hot vibrational states to the rate of the S_1/S_0 internal conversion process. For this, we build upon the transient absorption experiments performed by various groups, which have determined the kinetics of cooling of vibrational hot states in the S_1 state, generated as a result of the S_2/S_1 internal conversion.[27-31] The results of these experiments are used to further determine the dynamics of internal conversion initiating out of vibrationally hot states within the S_1 state potenial.

2. Experimental Section

Figure 1 shows a schematic potential energy diagram of β-carotene and the relevant double sided Feynman diagram of a time-resolved transient grating experiment (TG) applied to characterizing the kinetics of the internal conversion (IC) that couples the S_1 and electronic ground state of β-carotene. For the realization of this experimental scheme, 0.1 mM solutions of β-carotene in acetone were prepared in a rotating sample with a cell thickness of 0.5 mm. Gratings of S_2 state population were induced in the sample space by focusing two noncollinear pump lasers pulses ($\mathbf{k}_1$ and $\mathbf{k}_2$ in Figure 1, $\lambda_{pu} = 510$ nm, fwhm = 70 fs, 60 nJ) into the sample in resonance with the $S_2 \leftarrow S_0$ optical transition in β-carotene. The subsequent S_2/S_1 internal conversion allows for population flow into the S_1 state, generating a grating of S_1 state molecules. While the two pump pulses interact simultaneously with the sample, a third probe pulse ($\mathbf{k}_3$ in Figure 1, $\lambda_{probe} = 570-635$ nm, fwhm = 70 fs, 50 nJ) resolves the kinetics of the S_1 state with the help of a variable time delay, Δt, between the grating formation by the two pump pulses and the interrogation with the probe pulse. The probing of the S_1 state is accomplished by elastically scattering the probe pulse under Bragg conditions off the S_1 state population grating in resonance to the $S_n \leftarrow S_1$ optical transition in β-carotene. The transient grating signal ($\mathbf{k}_{TG}$ in Figure 1), scattered in the phase matched direction, $\mathbf{k}_{TG} = \mathbf{k}_1 - \mathbf{k}_2 + \mathbf{k}_3$ is directed into a monochromator and the spectral components of the signal are detected with a multichannel CCD detector. The intensity of the different spectral channels in the signal is recorded as a function of the delay time, Δt, between the two pump pulses, $\mathbf{k}_1$ and $\mathbf{k}_2$, and the probe pulse, $\mathbf{k}_3$. This allows for the observation of the population flow from the originally prepared S_2 state into the S_1 state through the S_2/S_1 IC, and the subsequent depopulation of the S_1 state by means of the S_1/S_0 IC. Because the S_2 state lies approximately 6000 cm^{-1} above the S_1 state, the S_2/S_1 IC prepares vibrationally hot modes in the S_1 state.[28] To monitor the population flow in different regions of the S_1 potential, the central wavelength of the probe pulse was varied from 570 to 635 nm to include spectral positions that lie red-shifted to the $S_n \leftarrow S_1$ transition.[32,33] Vibrational ground state modes can be monitored when the probe laser is in resonance with the S_1 absorption whereas red-shifting out of the absorption profile brings the probe laser pulse in resonance with vibrationally hot states of the S_1 potential.[34,35]

3. Results

In Figures 2 and 3, the signal intensity of the scattered probe pulse is plotted as a function of the delay time, Δt, between the two pump laser pulses that form the grating and the probe laser pulse scattered off this grating. Because the probe pulse is scattered elastically, a given spectral position in the signal corresponds to the spectral component of the probe pulse that interrogates the dynamics of the grating.[36-39] For an overview, the signals obtained by varying the probe pulse from $\lambda_{probe} = 570$ nm to 635 nm ($\tilde{\nu}_{probe} = 15\,950-16\,950$ cm^{-1}) are shown in panels A−D in Figure 2. These wavelengths lie exclusively in the red flank of the S_1/S_n transient absorption spectrum of β-carotene, which can readily be found in the literature for

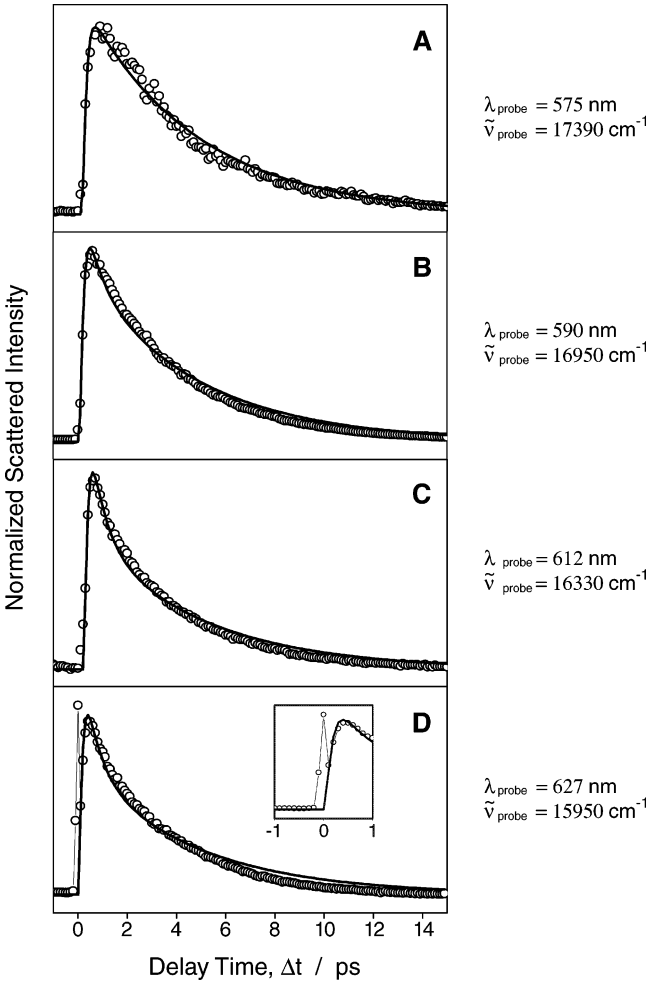

Figure 2. Scattered intensity of the probe pulse plotted as a function of the delay time, Δt. Panels A−D show the transient signal for different spectral positions of the probe laser. The experimental data points are shown as open circles and the theoretical fits are given as solid lines, using eq 1 with the parameters of model 1 listed in Table 1. The inset in panel D shows a time window that emphasizes the nonresonant scattering observed at this spectral position.

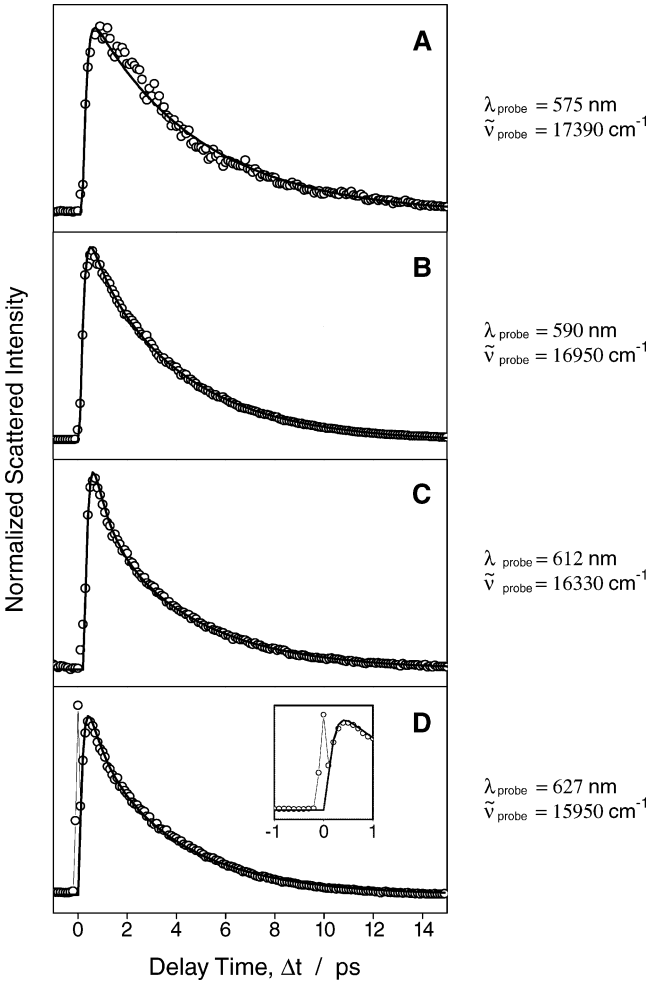

Figure 3. Scattered intensity of the probe pulse plotted as a function of the delay time, Δt. Panels A−D show the transient signal for different spectral positions of the probe laser. The experimental data points are shown as open circles and the theoretical fit as a solid lines, using eq 1 with the parameters of model 2 listed in Table 1. The inset in panel D shows a time window that emphasizes the nonresonant scattering observed at this spectral position.

comparison.[35] The experimental data points (displayed as open circles in the plot) show the dynamics observed at the maximum signal intensity for the four different central wavelengths of the probe pulse. The dynamics were further analyzed at the blue and red side of the fwhm in the spectral profile of the signal.

From a first qualitative comparison of the curves in Figure 2, it can be seen that the transient signal shows a dependency on the spectral position at which the signal is observed. The first evident feature in panels A−D is an intense peak centered around $\Delta t = 0$ ps that is observed for a detection at 627 nm (15 950 cm^{-1}) in panel D and not seen in the other transient signals. This peak is attributed to the nonresonant scattering of the probe pulse from the grating formed by the electric field of the two pump pulses that is independent of an electronic resonance in the chromophore of the sample.[40,41] The peak is only observed for delay times during which the two pump pulses and the probe pulse interact simultaneously with the sample and shows a temporal profile that corresponds to the convolution of these three laser pulses. The scattering mechanism is in contrast with the resonant scattering from the grating of electronically excited molecules possessing an electronic transition that is in resonance with the frequency of the probe pulse. This resonant scattering can be observed for delay times of $\Delta t \geq 100$ fs at all the spectral positions of the signal. In the latter case, the pump pulses prepare a grating of a transient population and the probe pulse utilizes the $S_n \leftarrow S_1$ transition for the resonant scattering.

The lack of a nonresonant peak for the transients in panels A−C in Figure 2 is surprising at first because the blue-shift wavelengths of the probe pulse, used for the transients in panels A−C should lead to a stronger nonresonant scattering effect. The missing nonresonant peak centered around $\Delta t = 0$ can therefore only be the result of a change in the ratio between the nonresonant signal and the resonant signal observed at $\Delta t \geq 100$ fs. In the progression of Figure 2 from panel A to D, the spectral position of the probe laser is shifted further toward, and eventually out of, the red flank of the S_1 state absorption. This change in the electronic resonance conditions for the probe pulse causes a decrease in the intensity of the resonant signal in relation to the nonresonant contribution. For the transients recorded between 575 and 612 nm (17 390 and 16 330 cm^{-1}) in panels A−C, the ratio between resonant and nonresonant effects is overwhelmingly in favor of the resonant signal, which makes the nonresonant contribution diminish to the point of not being apparent. For the transient recorded at 627 nm (15 950 cm^{-1}), the decreasing resonant signal allows for the nonresonant effect to become noticeable. The effect was further verified for probe wavelengths up to 690 nm (14493 cm^{-1}), which are

shifted even further into the red. For these probe wavelengths, an intense nonresonant contribution can be seen that is highly convoluted with the very weak resonant signal, making the evaluation of the resonant data difficult for these detection wavelengths.

To evaluate the resonant transient data, a model was formulated that includes the possible population and depopulation channels for the region of the S_1 potential that is monitored by the probe pulse. The S_2/S_1 internal conversion is assumed to be the only mechanism with which the S_1 state is populated, the time constant being, τ_{S_2/S_1}.[42] For molecules in the vibrational ground state of the S_1 potential, the S_1/S_0 internal conversion is assumed to be the only channel of depopulation and this process is characterized with the time constant, τ_{S_1/S_0}. Fluorescence as a decay channel for S_1 state molecules can be neglected because the $S_1 \leftarrow S_0$ optical transition is symmetry forbidden. For wavelengths of the probe laser that are red-shifted to the S_1 state absorption, it is postulated that vibrationally hot states are also interrogated by the probe laser pulse. In this case, two possible decay channels are postulated that allow molecules to leave the region of the S_1 potential that is interrogated by the probe laser. The first channel is the S_1/S_0 internal conversion taking place out of vibrationally hot states. The second channel is given by vibrational cooling due to system-bath coupling, resulting in energy transfer to solvent molecules. The cooling processes are described with a global time constant for all modes, τ_{cool}.

The population flow into the S_1 state is characterized by the time constant τ_{S_2/S_1} of the S_2/S_1 internal conversion. This channel of population is coupled with the multiple mechanisms of depopulation, which are characterized by the time constants for the S_1/S_0 internal conversion, τ_{S_1/S_0}, and the global time constant for vibrational cooling τ_{cool}. The later two decay channels are not coupled. These assumptions for the S_1 state kinetics in combination with the time dependency of a transient grating signal result in the following model for the resonant transient data:[21,47]

$$I_{TG}(\Delta t) = |(1 - e^{-\Delta t/\tau_{S2/S1}})[Ae^{-\Delta t/\tau_{cool}} + (1 - A)e^{-\Delta t/\tau_{S1/S0}}]|^2 \quad (1)$$

The model above possesses four variable parameters describing the transient data, consisting of τ_{S_2/S_1}, τ_{cool}, τ_{S_1/S_0}, and A, the amplitude factor, which describes the distribution between cooling and the S_1/S_0 internal conversion as a decay channel out of the probe window. A free fit of all the parameters in eq 1 would prove difficult because the multitude of variables makes the determination of a minimum for the least-mean-squares fit difficult. Due to this, data from the literature are used to estimate the time constants of the processes involved in the kinetics. Macpherson et al. performed solvent-dependent measurements of the S_2/S_1 internal conversion using fluorescence up-conversion of the S_2 state fluorescence and determined a time constant of $\tau_{S_2/S_1} = 134$ fs for β-carotene dissolved in acetone.[28] In the group of de Silvestri, the vibrational cooling effects in the S_1 state of β-carotene after the S_2/S_1 internal conversion were characterized with a global time constant of $\tau_{cool} = 623$ fs[29] and transient infrared absorption measurements in the group of Sundstrøm characterize the cooling in the S_1 state after the S_2/S_1 internal conversion in analogue carotenoids with a very similar time constant of $\tau_{cool} = 750$ fs.[30] The solvent effect on the S_1/S_0 internal conversion was explored with transient absorption which allows for τ_{S_1/S_0} in acetone to be estimated with 9.2 ps.[31] By using the time constants summarized in Table 1 under model 1 to fit the resonant signal from the transient grating data, only the amplitude factor, A, is left as a free variable in eq 1. The distribution between the two channels leading to a decay of the signal is characterized by directly assigning the cooling process the factor A and the S_1/S_0 internal conversion the corresponding amplitude of $(1 - A)$. This allows for the expression $(A \cdot 100)$ to describe the percentage of vibrational states that take the pathway of vibrational cooling to leave the region of the S_1 potential interrogated by the probe laser.

TABLE 1: Summary of the Two Models for the Transient Grating Data Using Equation 1[a]

parameter	model 1	model 2
$\tau_{S2/S1}$[28]	134 fs	134 fs
τ_{cool}[29,30]	700 fs	700 fs
$\tau_{S1/S0}$[31]	9.20 ps	variable (panel C, Figure 5)
A	variable (panel A, Figure 5)	variable (panel B, Figure 5)

[a] The models differ with respect to the parameters that are fit as free variables and parameters that are fixed with literature values.

The model can directly be applied to the transients in panels A−C in Figure 2 that show a negligible nonresonant contribution at $\Delta t = 0$. For the transient in panel D, which exhibits a strong nonresonant contribution, a deconvolution of the resonant and nonresonant signal must be carried out because the kinetic model only describes the resonant scattering out of the S_1 state. The nonresonant contribution is characterized by replacing the sample with a glass platelet and recording the transient signal under analogue experimental conditions. Because the glass platelet shows no resonant response, the transient signal attained in this manner gives the temporal profile. The nonresonant profile acquired from the glass platelet corresponds to the convolution of all three lasers involved in the optical process. This nonresonant profile from the glass platelet is deconvoluted from the transient data points, and the resulting, deconvoluted data set is fit with the model described above, where the data points remaining from the nonresonant profile are not included in the fitting process. To directly compare the quality of the fit to the transient data that did not require the deconvolution process, the theoretical curve generated out of the fit to the deconvoluted data set is convoluted with the nonresonant profile from the glass platelet. This convoluted fit curve is shown as a solid line with the original data in panel D of Figure 2.

The fits to the experimental data are shown as solid lines in Figure 2. The fits show that using the fixed time constants of model 1 for eq 1 gives a good first approximation of the experimental data. The amplitude factors, A, determined from the fit are plotted in the form of $(A \cdot 100)$ as a function of the spectral position of the probe pulse in panel A of Figure 5. An interpretation of the tendency observed in the amplitude factor, A, as a function of the spectral position of the probe will be given in the following section. Despite the relatively good approximation of the transient data with the respective amplitude factors, deviations of the fit in specific regions of the experimental data call for a modification of the model. Although the transient at 17 390 cm^{-1} shows the best agreement with the model, the deviations from the experimental data increase with a further red-shift of the probe pulse. This growing deviation can be seen as an overestimated amplitude A for the decay channel of cooling. The overestimated amplitude factor is the result of this fit variable overcompensating for a changing decay time of either the cooling process described by τ_{cool} or the S_1/S_0 internal conversion given by τ_{S_1/S_0}. To further illustrate this growing deviation as the probe is red-shifted, the fit curves are subtracted from the experimental data. The resulting curves are plotted in Figure 4 for the probe at 590 nm (16 950 cm^{-1}, panel

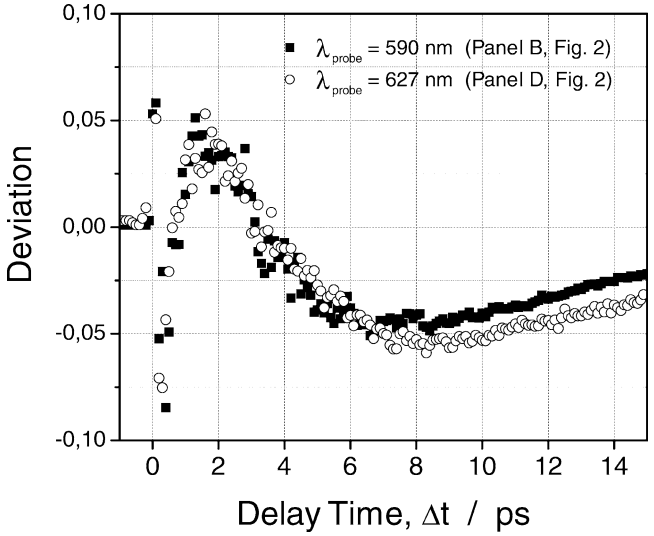

Figure 4. Curves obtained by subtracting the theoretical fit using model 1 from the experimental data shown in Figure 2. The curves are plotted as open circles for the probe at 590 nm (16 950 cm^{-1}, panel B of Figure 2) and as filled squares for the probe at 627 nm (15 950 cm^{-1}, panel D of Figure 2). The chosen wavelengths of the probe correspond to the measurements performed in the middle and the red end of the spectral range used for the probe pulse. The plots illustrate the increasing deviation of the experimental data to fit curves using model 1 in the region of the transient between 6 and 15 ps that is characterized by the S_1/S_0 internal conversion. For details see text.

B of Figure 2) and at 627 nm (15 950 cm^{-1}, panel D of Figure 2), which correspond to the measurements preformed in the middle and the red end of the spectral range used for the probe pulse. The deviations from the experimental data are particularly evident, in the region between $6 \leq \Delta t \leq 15$ ps, which are characterized by τ_{S_1/S_0}. Because the deviations are larger and increase with red-shifted probe wavelengths primarily in the region characterized by the decay channel of S_1/S_0 internal conversion, it is assumed that this parameter leads to the deviation of the fits from the experimental data. Various experiments in the literature confirm this, e.g., Mathies et al.,[48] analyzed the vibrational relaxation in β-carotene by means of Stokes and anti-Stokes resonance Raman spectroscopy. They found that the vibrational relaxation in the S_1 state is complete within 2 ps and therefore much faster than the S_1/S_0 internal conversion. This supports the tendency observed when using model 1.

To improve the quality of the fit to the experimental data, the fit procedure is modified so that a variable time constant for the S_1/S_0 internal conversion is taken into consideration for the different regions of the S_1 potential that were probed. For this, the model described in eq 1 is again applied in the fit procedure and, consistent with model 1 presented above, the time constants for the S_2/S_1 internal conversion and the cooling process are fixed with the literature values for τ_{S_2/S_1} and τ_{cool}. Deviating from the first model, we now use the amplitude factor A and the time constant for the S_1/S_0 internal conversion, τ_{S_1/S_0}, as fit parameters. The employed numerical values of the latter are summarized in Table 1 under model 2. Transients that require deconvolution of the resonant and nonresonant contributions of the signal are fit with the same procedure as described above. The obtained fits to the transient data are shown as solid lines in panels A−D in Figure 3. Furthermore, the amplitude factor, A, as well as the time constant, τ_{S_1/S_0}, obtained by using model 2 is plotted as a function of the spectral position of the probe in panel B and C of Figure 5. By allowing τ_{S_1/S_0} to fit freely, the second model shows excellent agreement with the

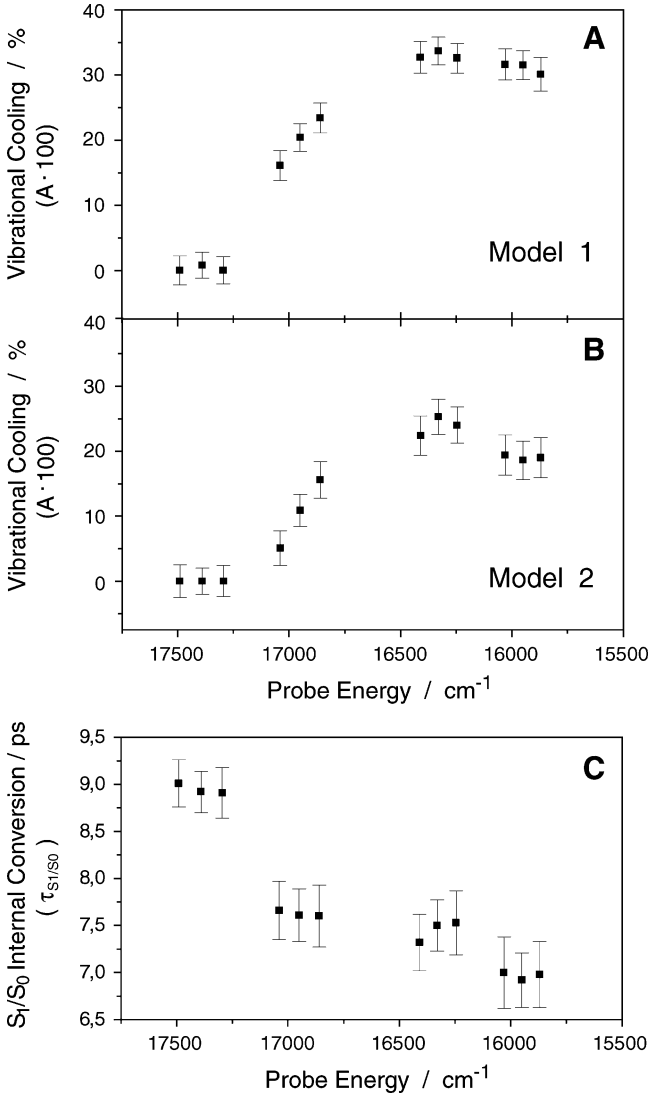

Figure 5. Parameters obtained from the fits to the experimental data shown in Figures 2 and 3 using eq 1. (A) Percentage cooling as a function of the spectral position of probe pulse using model 1 (see Table 1). (B) Percentage cooling as a function of the spectral position of probe pulse using model 2 (see Table 1). (C) Time constant, τ_{S_1/S_0}, for the respective internal conversion as a function of the probe energy using model 2. For details see the text.

experimental data. In Figure 5 a comparison of the values for amplitude factor A obtained from each model shows that the general tendency of this factor, seen as a steplike increase toward red-shifted detection positions, remains the same for both models. It should also be noted that the values obtained from the fit for A at $\tilde{\nu}_{probe} = 17\,490$, 17 390, and 17 295 cm^{-1} using both models are in the range between $0\% \leq (A \cdot 100) \leq 0.8\%$, yet the deviation shows also negative values. They arise when the amplitude factor for the cooling time compensates for the transient data deviating from the fixed literature values of $\tau_{S_2/S_1} = 134$ fs and $\tau_{S_1/S_0} = 9.2$ ps. The negative values for A were included in the error of A to illustrate that the fixed literature values are only an approximation to the data obtained with the transient grating technique in this work and to further show the limited accuracy with which A can be determined with this fit strategy.

4. Discussion

By fitting the experimental data with the second model, it was possible to characterize the distribution between vibrational

cooling and internal conversion as a decay channel in the S_1 state with the amplitude factor, *A*, and, furthermore, determine the time constant for the S_1/S_0 internal conversion as a function of the spectral position of the probe pulse. The results of the fits described in the previous section are summarized in Figure 5.

The characterization of the amplitude factor, *A*, gives insight into the region of the S_1 potential energy surface that is interrogated when the probe laser is red-shifted toward and eventually out of the red flank of the S_1 state absorption. The S_2 state lies approximately 6000 cm^{-1} above the vibrational ground state of the S_1 state for β-carotene in acetone and this excess energy is transferred into the vibrational modes of the S_1 state after the S_2/S_1 internal conversion. This generates vibrationally hot molecules in the S_1 state that undergo cooling processes.[29,49] The energy necessary for a resonance with the $S_n \leftarrow S_1$ optical transition is insufficient for the vibrational ground state molecules in the S_1 state when the probe laser is red-shifted out of the absorption profile of the S_1 state. This forces the probe to interrogate energetically higher lying vibrational states that can still utilize the $S_n \leftarrow S_1$ optical transition, because the excess vibrational energy compensates for the red-shifted probe pulse. A similar experimental scheme was realized in the group of Sundstrøm[35] with transient absorption measurements of the S_1 state in β-carotene and by Duppen et al. with two color photon echos in pentacene.[36]

The behavior of the amplitude factor, *A*, as a function of the spectral position of the probe laser, displayed in Figure 5, confirms that the strategy of spectrally red-shifting the probe for the interrogation of vibrationally hot states in the S_1 state shows the desired effect. The percentage cooling as a decay channel out of the region in the S_1 state potential being probed, given by (A·100), shows a strong increase of up to 25% (model 2, in Figure 5) for the red spectral positions between 16 500 and 15 500 cm^{-1}. This is in contrast to the absence of the fast decay channel of cooling for the blue spectral region of the probe from 17 500 to approximately 17 250 cm^{-1}. Here, the probe laser primarily interrogates vibrational ground state molecules when the color is tuned to a spectral region that is in strong resonance with the $S_n \leftarrow S_1$ optical transition. Important to further note about the behavior of the amplitude factor, *A*, is the consistency between the tendency in the fit values for (A·100) extracted from different spectral positions of a single measurement and the general tendency of (A·100) when the central wavelength of the probe laser is shifted. Here, the sharp slope in the values extracted form three spectral positions within the spectral profile of the probe laser centered around 16 950 cm^{-1} follows the general tendency of (A·100) observed over the full spectral region probed.

By establishing the probing of vibrationally hot states in the S_1 potential via the contribution of cooling processes to the transient data, it is possible to discuss the behavior of the time constant for the S_1/S_0 internal conversion, τ_{S_1/S_0}, as a function of the spectral position of the probe laser (panel C of Figure 5). In the previous section, the transient data for the different spectral positions of the probe were characterized with a first model that used fixed literature values for all the time constants involved in the S_1 state kinetics. This first model was presented to demonstrate that the fixed values for τ_{S_2/S_1}, τ_{cool}, and τ_{S_1/S_0} show good agreement for the probe between 17 500 and 17 250 cm^{-1} (panel A, Figure 2) that are in strong resonance with the $S_n \leftarrow S_1$ optical transition. For red-shifted probe energies, where vibrationally hot states are interrogated and a vibrational cooling noticeably contributes to the kinetics observed, the first model is inadequate for describing the population flow in the vibrationally excited states, if the varying contribution of the cooling process via the amplitude factor, *A*, is the only parameter considered in the fit. The obvious deviations of the fit using model 1 (panels B−D, Figure 2 and Figure 4) call for the revised model 2, which allows for a variable fit of the amplitude factor, *A*, as well as the time constant describing the S_1/S_0 internal conversion, τ_{S_1/S_0}. This revision in the fit procedure allows the transient data for all spectral positions to show good agreement with the model (see panels A−D, Figure 3).

When the time constant for the S_1/S_0 internal conversion is varied in model 2, a clear tendency of τ_{S_1/S_0} can be observed as a function of the spectral position of the probe pulse (panel C of Figure 5). The plot of τ_{S_1/S_0} clearly shows that the S_1/S_0 internal conversion begins in the blue-shifted region with a value of $\tau_{S_1/S_0} \approx 9.0$ ps and becomes faster for the red-shift spectral region, reaching a minimum in the time constant of approximately 7 ps in the region between 16 500 and 15 500 cm^{-1}. A comparison of the behavior of the amplitude factor, *A*, and the time constant, τ_{S_1/S_0}, as a function of the spectral position of the probe in panels B and C in Figure 5, shows a strong correlation between both variables. Here, *A* and τ_{S_1/S_0} show a sharp change in their values in the spectral region between 17 250 and 16 500 cm^{-1} that become constant in the region from 16 500 to 15 500 cm^{-1}. On the basis of this strong correlation, it is postulated that vibrationally hot states that are interrogated with a red-shifted probe pulse undergo a faster internal conversion than vibrational ground state modes in the S_1 potential. Because the contribution of vibrational cooling as a decay channel, given by *A*, is a measure for the amount of vibrationally excited states contributing to the total signal, it can be concluded that the decrease in the time constant for the S_1/S_0 internal conversion, is the result of vibrationally excited states possessing a faster time constant for the S_1/S_0 internal conversion.

Because a single time constant, τ_{S_1/S_0}, is used in the fit procedure, the values extracted from the fit represent an integral time constant for all vibrational states contributing to the signal (including vibrationally excited as well as vibrational ground state modes in the S_1 potential). It would be possible to attempt a disentanglement of the time constants for vibrational excited states and vibrational ground state modes by modifying eq 1 to include two separate time constants for both cases. Attempts at these types of fits have shown that the two time constants for the internal conversion of vibrationally hot and cold modes do not show adequate separation in their values. Therefore, the experiments presented here only allow for the qualitative result that vibrationally hot states in the S_1 state undergo an internal conversion to the electronic ground state with a faster time constant than the vibrational ground state modes.

The faster S_1/S_0 internal conversion for vibrationally excited modes in the S_1 state can be the result of a variety of parameters. Advantageous Franck−Condon factors or coupling constants for the excited vibrational modes as well as the higher energy for a tunneling process between the two participating electronic states or overcoming of energy barriers on the S_1 state potential can result in a faster internal conversion for the vibrationally hot molecules.[4−6,8−10,50,51] The experiments presented here do not allow for an identification of the effect that results in the faster internal conversion because the participating potentials are not characterized sufficiently. It is also important to consider that the contribution of vibrationally excited states to the overall population transfer between the S_1 and S_0 potential will be small

because this process is in competition with the much faster process of vibrational cooling.

The last important property of the experimental data characterized by the behavior of the amplitude factor, *A*, and the time constant, τ_{S_1/S_0}, is the steplike change as a function of the spectral position of the probe laser. Rather than a continuous change in these two parameters as the spectral position of the probe is red-shifted, both parameters show a jump in a relatively small spectral region of the probe to a value that stays consistent for further change in the probe energy. A sudden change in a molecular parameter as a function of energy can often be associated with the quantum states in the molecular system. In the following, the steplike behavior of *A* and τ_{S_1/S_0} (panels B and C, in Figure 5, respectively) is correlated to quantum spacing of vibrational modes given by the S_1 state Raman spectrum and the particular sensitivity of the $S_n \leftarrow S_1$ optical transition to a specific Franck−Condon active mode.[49] The jump in the values for amplitude factor, *A*, and the time constant, τ_{S_1/S_0}, takes place in a spectral region between approximately 17 300 and 16 300 cm^{-1}, which corresponds to an energy difference of $\tilde{\nu} \approx 1000$ cm^{-1}. This tendency in the S_1 kinetics was attained by utilizing the $S_n \leftarrow S_1$ optical transition, which shows a vibronic structure with an estimated energy spacing of $\Delta\tilde{\nu} \approx 1150$ cm^{-1} in the transient absorption spectrum at 20 K recorded by Kispert and co-workers.[32] The structure shows that the $S_n \leftarrow S_1$ transition possesses a Franck−Condon active mode or modes, which make this optical transition sensitive to the quantum spacing of particular vibrational modes. With the considerations presented above, the steplike behavior of the amplitude factor, *A*, and the time constant, τ_{S_1/S_0}, is eventually the result of the probe pulse switching from the interrogation of the vibrational ground state to the probing of vibrationally excited state modes. The fast change in ratio between the resonant and nonresonant signals (seen in the appearance of the nonresonant peak at $\Delta t = 0$ in panel D of Figure 3) in combination with the lack of a further steplike change in the behavior of *A* and τ_{S_1/S_0} for the spectral region between 16 000 and 15 500 cm^{-1} (panels B and C, in Figure 5) could be the result of extremely poor Franck−Condon factors for the probing of higher vibrational quantum states. Despite this, the varying resonance conditions of the probe for different vibrational modes in different quantum states of the S_1 state and the poor characterization of the S_n states make the interpretation of the steplike behavior in the amplitude factor, *A*, and the time constant of internal conversion, τ_{S_1/S_0}, as a function of the spectral position of the probe laser extremely difficult. Due to this, the model of a jump in the interrogation of the vibrational modes of the S_1 state should only be seen as one possible conclusion.

5. Conclusion

With the interpretation of the experimental data presented above, it could be shown that transient gratings are an effective experimental method for investigating the kinetics in excited electronic dark states. The kinetics of ground state versus vibrationally excited state modes engaging in the internal conversion between the S_1 and electronic ground state could be differentiated and the interrogation of an electronic potential in areas that show very small absorption cross sections was possible. This is due to the high sensitivity of this spectroscopic method given by the background free signal that requires no reference subtraction. In the case of β-carotene presented here, it could be shown that the strategy of red-shifting the probe laser out of an electronic resonance allows for the interrogation of vibrationally exited states within the S_1 potential. The distribution between cooling processes and internal conversion as a decay channel in vibrationally excited modes was determined. The high sensitivity of the transient grating technique with respect to the transient population gives a signal quality that further allows for the kinetics of vibrationally hot versus vibrational ground state modes to be differentiated. Due to this, a faster rate for the S_1/S_0 internal conversion for vibrationally excited states could be characterized.

Acknowledgment. This work was funded by the Deutsche Forschungsgemeinschaft (Schwerpunktprogramm "Femtosekunden-Spektroskopie elementarer Anregungen in Atomen, Molekülen und Cluster," Projekt KI 202/14-3 and EN 241/5-3.) We also acknowledge financial support from the Fonds der Chemischen Industrie.

Note Added after ASAP Posting. This article was released ASAP on 9/06/2003. A paragraph was inadvertently deleted during production. This paragraph is now cited as ref 42 and the following references (43 through 51) have been renumbered. The correct version was posted on 9/12/2003.

References and Notes

(1) Born, M.; Oppenheimer, R. *Ann. Phys.* **1927**, *84*, 457−484.
(2) Born, M.; Heisenberg, W. *Ann. Phys.* **1924**, *74*, 1−31.
(3) Schroedinger, E. *Phys. Rev.* **1926**, *28*, 1049−1070.
(4) Englman, R.; Jortner, J. *Mol. Phys.* **1970**, *18*, 145−164.
(5) Domcke, W.; Köppel, H.; Cederbaum, L. S. *Mol. Phys.* **1981**, *43*, 851−875.
(6) Siebrand, W.; Zgierski, M. Z. *J. Chem. Phys.* **1981**, *75*, 1230−1238.
(7) Bersuker, I. B.; Polinger, V. Z. *Vibronic Interaction in Molecules and Crystals*; Springer Series: Chemical Physics; Springer: Berlin, 1985; Vol. 49.
(8) Bernardi, F.; Olivucci, M.; Robb, M. A. *Chem. Soc. Rev.* **1996**, 321−328.
(9) Stock, G.; Domcke, W. *Adv. Chem. Phys.* **1997**, *100*, 1−169.
(10) Bixon, M.; Jortner, J. *J. Chem. Phys.* **1997**, *107*, 1470−1482.
(11) Blanchet, V.; Zgierski, M. Z.; Seideman, T.; Stolow, A. *Nature* **1999**, *401*, 52−54.
(12) Schoenlein, R. W.; Peteanu, L. A.; Mathies, R. A.; Shank, C. V. *Science* **1991**, *254*, 412−415.
(13) Wang, Q.; Schoenlein, R. W.; Peteanu, L. A.; Mathies, R. A.; Shank, C. V. *Science* **1994**, *266*, 422−424.
(14) Scholes, G. D.; Fleming, G. R. *J. Phys. Chem. B* **2000**, *104*, 1854−1868.
(15) Hahn, S.; Stock, G. *J. Phys. Chem. B* **2000**, *104*, 1146−1149.
(16) Zewail, A. H. *Femtochemistry: Ultrafast Dynamics of the Chemical Bond*; World Scientific: Singapore, 1994; Vols. I and II.
(17) Manz, J., Wöste, L., Eds. *Femtosecond Chemistry*; VCH: Weinheim, 1995.
(18) Chergui, M., Ed. *Femtochemistry*; World Scientific: Singapore, 1996.
(19) Shen, Y.-R. *The Principles of Nonlinear Optics*; Wiley: New York, 1984.
(20) Mukamel, S. *Annu. Rev. Phys. Chem.* **1990**, *41*, 647−681.
(21) Mukamel, S. *Principles of Nonlinear Optical Spectroscopy*; Oxford University Press: New York, 1995.
(22) Joo, T.; Albrecht, A. C. *Chem. Phys.* **1993**, *173*, 17−26.
(23) Lee, D.; *Advances in Infrared and Raman Spectroscopy*; Albrecht, A. C. In Clark, R. J. H., Hester, R. E., Eds.; J. Wiley & Sons: Chichester, U.K., 1985; Vol. 12, pp 179−213.
(24) Lee, D.; Albrecht, A. C. In *Advances in Chemical Physics*; Prigogine, I., Rice, S. A., Eds.; John Wiley & Sons: Chichester, U.K., 1993; pp 43−87.
(25) Koyama, Y.; Mukai, Y. In *Biospectroscopy*; Clark, R. J. H., Hester, R., Eds.; Biomolecular Spectroscopy: Part B; John Wiley & Sons: New York, 1993; Vol. 21, pp 49−116 (advances in spectroscopy edition).
(26) Frank, H. A.; Cogdell, R. J. *Photochem. Photobiol.* **1996**, *63*, 257−264.
(27) Shreve, A. P.; Trautman, J. K.; Owens, T. G.; Albrecht, A. C. *Chem. Phys. Lett.* **1991**, *178*, 89−96.
(28) Macpherson, A. N.; Gillbro, T. *J. Phys. Chem. A* **1998**, *102*, 5049−5058.
(29) Cerullo, G.; Lanzani-Rossi, G.; DeSilvestri, S. *Phys. Rev. B* **2001**, *63*, 241104/1−241104/4.
(30) Polivka, T.; Zigmantas, D.; Frank, H. A.; Bautista, J. A.; Herek, J. L.; Koyama, Y.; Fujii, R.; Sundström, V. *J. Phys. Chem. B* **2001**, *105*, 1072−1080.

(31) He, Z.; Gosztola, D.; Deng, Y.; Gao, G.; Wasielewski, M. R.; Kispert, L. D. *J. Phys. Chem. B* **2000**, *104*, 6668−6673.

(32) Wasielewski, M. R.; Johnson, D. G.; Bradford, E. G.; Kispert, L. D. *J. Chem. Phys.* **1989**, *91*, 6691−6697.

(33) Nagae, H.; Kuki, M.; Zhang, J.-P.; Sashima, T.; Mukai, Y.; Koyama, Y. *J. Phys. Chem.* **2000**, *104A*, 4155−4166.

(34) Polivka, T.; Zigmantas, D.; Frank, H. A.; Bautista, J. A.; Herek, J. L.; Koyama, Y.; Fujii, R.; Sundström, V. *J. Phys. Chem. B* **2001**, *105*, 1072−1080.

(35) Billsten, H. H.; Zigmantas, D.; Sundström, V.; Polivka, T. *Chem. Phys. Lett.* **2002**, *355*, 465−470.

(36) Duppen, K.; Weitekamp, D. P.; Wiersma, D. A. *Chem. Phys. Lett.* **1984**, *108*, 551−554.

(37) Wiersma, D. A.; Duppen, K. *Science* **1987**, *237*, 1147−1154.

(38) Eichler, H. J.; Gunter, P.; Pohl, D. W. *Laser Induced Dynamics Gratings*; Springer: Berlin, 1986.

(39) Laubereau, A. In *Ultrafast Laser Pulses and Applications*; Kaiser, W., Ed.; Springer: Berlin, 1988; Vol. 60, pp 35−111 (topics in applied physics edition).

(40) Kohles, N.; Aechtner, P.; Laubereau, A. *Opt. Commun.* **1988**, *65*, 391−396.

(41) Ferwerda, H. A.; Terspsta, J.; Wiersma, D. A. *J. Chem. Phys.* **1989**, *91*, 3296−3305.

(42) The precise mechanism that transfers population between the S_2 and S_1 states is still unclear. There must be a sequential internal conversion of the S_2 state via one ($1B^-_u$) or two ($3A^-_g$, $1B^-_u$) intermediate states.[43−46] However, due to the fact that the lifetime of these intermediate states is extremely short, vibrational cooling within these states only makes a negligible contribution to the dynamics. This makes the transition from the S_2 to the S_1 state via other electronic states virtually isoenergetic. Furthermore, the pump lasers are kept constant in their wavelength, which allows for the assumption that the mechanism with which the S_1 state is populated remains constant for all measurements. Additionally, the probe process is only sensitive to the population within the S_1 state and thus insensitive to the mechanism with which the S_1 state is populated.[35]

(43) Sashima, T.; Koyama, Y.; Yamada, T.; Hashimoto, H. *J. Phys. Chem. B* **2000**, *104*, 5011.

(44) Fujii, R.; Ishikawa, T.; Koyama, Y.; Taguchi, M.; Isobe, Y.; Nagae, H.; Watanabe, Y. *J. Phys. Chem. A* **2001**, *105*, 5348.

(45) Furuichi, K.; Sashima, T.; Koyama, Y. *Chem. Phys. Lett.* **2002**, *356*, 547.

(46) Fujii, R.; T..; Watanabe, Y.; Koyama, Y.; Zhang, J.-P. *Chem. Phys. Lett.* **2003**, *369*, 165.

(47) Zinth, W.; Kaiser, W. In *Ultrafast Laser Pulses and Applications*; Kaiser, W., Ed.; Springer: Berlin, 1988; Vol. 60, pp 235−277 (topics in applied physics edition).

(48) McCamat, D. W.; Kim, J. E.; Mathies, R. A. *J. Phys. Chem. A* **2002**, *106*, 6030−6038.

(49) Nagae, H.; Kuki, M.; Zhang, J.; Sashima, T.; Mukai, Y.; Koyama, Y. *J. Phys. Chem. A* **2000**, *104*, 4155−4166.

(50) Freed, K. F. *Radiationless Process in Molecules and Condensed Phases*; Springer: Berlin, 1976; pp 23−168.

(51) Klessinger, M. *Angew. Chem., Int. Ed. Engl.* **1995**, *34*, 549−551.